

Experimental Results and Theoretical Comparison Obtained from a Rectangular Two-Channel Dielectric Wakefield Accelerator Experiment

S.V. Shchelkunov^[1], T.C. Marshall^[2], G. Sotnikov^[3], J.L. Hirshfield^[1,2], Wei Gai^[4],
M. Conde^[4], J. Power^[4], D. Mihalcea^[4], Z. Yusof^[4]

1)Yale University, New Haven, CT 06511, USA; 2) Omega-P, Inc, New Haven, CT 06510, USA; 3) NSC Kharkov Institute of Physics and Technology, 61108 Kharkov, Ukraine; 4) Argonne National Laboratory, Argonne, IL, 60439,USA

Abstract: We have obtained experimental results from a two-channel, cm-scale, rectangular dielectric-lined wakefield acceleration module that operates at ~30GHz and has a high transformer ratio (~12:1). The accelerated bunch is continuously energized in the secondary vacuum channel by a drive bunch in the primary channel via Cherenkov radiation exchange. Recent experiments are described providing results that agree well with theory model predictions. The observed energy gain or loss, transverse deflection, and changes in the test bunch density distribution are analyzed and are well understood.

Keywords: wakefield, two-channel, transformer ratio, dielectric-lined, acceleration

PACS: 41.75.Lx, 41.60.-m, 41.60.Bq

I. Introduction

A steadily growing interest in the accelerator community toward exploration of dielectric -loaded single- or multiple- channel structures that can support wakefields driven by either a single electron bunch or a train of bunches has provided a strong incentive for the research which we report below.

A variety of configurations was investigated or is being explored by different groups [1-27]. Expectations are [2, 3] that larger magnitudes of surface fields, compared with metal structures, can be tolerated by dielectric-lined structures. Wakefields also can be spatially localized by a virtue of a correctly chosen design, and this feature combined with the fact that wakefields move at near-light velocity in a vacuum channel surrounded by dielectric ensures that each spot of the adjacent dielectric surface is subjected to high field magnitudes for only a brief moment of time, thereby reducing the likelihood for breakdown and damage.

Our group and collaborators have investigated a rectangular two-channel dielectric-lined accelerator module that supports wakefields having frequencies of a few tens of GHz. The motivation behind using two-channel structures comes from a simple observation that a single-channel dielectric-lined module has a limitation [4-7] for achieving high transformer ratio [TR] unless provisions are made to drive them with bunch trains whose individual bunches have charges conforming to prescribed rules [8-11]. Moreover, if a single-channel structure is driven by a single drive bunch, a carefully profiled bunch distribution is needed within this bunch to achieve a TR above 2:1. On the other hand, two-channel modules can deliver a high TR without imposing any complex

set of requirements on the drive bunch or drive train. In two-channel structures, a redistribution of wakefields is possible so as to cause the acceleration gradient in one of the channels [hence referred to as the test or acceleration channel] to be much higher than the deceleration gradient in the other channel [normally referred to as the drive channel]. However, it should not be forgotten that achieving high TR is subject to limitations dictated by bunch stability requirements for both the accelerated and drive bunches, or drive trains [1, 12-14]. Recently, we have explored a more symmetrical version of the compact two-channel device, the coaxial dielectric wakefield accelerator [12 & 15]; in this device there are no lateral forces on the test bunch to zero order.

Here, we provide the comparison of the experimental results with the theory model predictions. To the best of our knowledge, this is the first experiment, to test a two-channel dielectric-lined wakefield device contained in one composite structure.

The goal of the experiment was to excite the structure with a single drive bunch [with well known parameters] that moves within and is well aligned with the drive channel [Fig.1], and to probe the wakefield set up by its passage in the test channel using a test bunch, also with well known parameters. The delay between bunches was adjusted to probe the fields at different distances behind the drive bunch. As theory finds, the dynamics of the test bunch is dictated mostly by two forces, F_z and F_x that arise because of the corresponding components of the wakefield. While the first force changes the test bunch energy, the second one kicks the bunch horizontally. Both effects are well observed and quantified on the spectrometer screen, thereby allowing one to find experimentally the strength of the wakefields in a straightforward manner and later make comparisons with the model predictions. Thereby, we shall provide evidence that the simulation and analytical tools and models are adequate, and our understanding of the interaction between the wakefields and bunches is valid.

The structure cross-section is shown in Fig.1

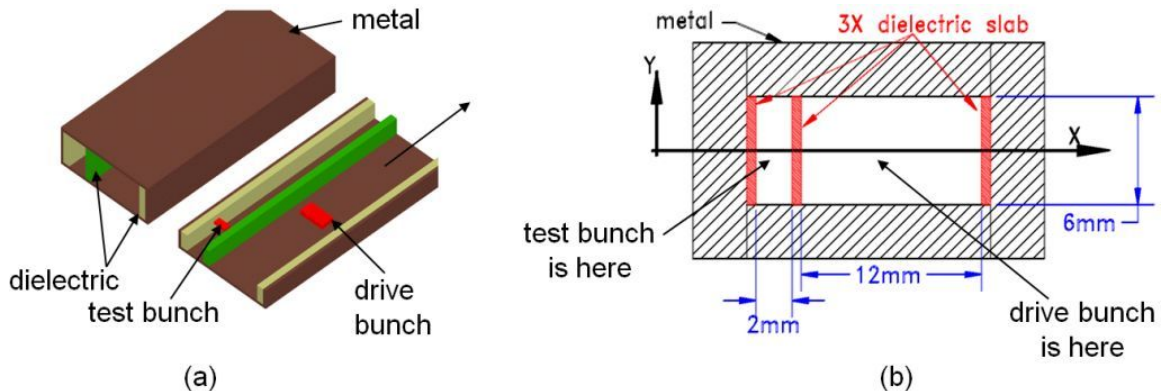


Fig.1: (a) Module schematic, and (b) cross-section of the apparatus with the channel dimensions. Both channels are 10cm long; the entire apparatus is longer because of a stainless steel mask in front to collimate the bunches. The dielectric is cordierite with the dielectric constant of 4.76; the slabs [manufactured by Euclid Techlabs LLC] have thicknesses [from left-to-right] 1.25mm, 2.3 and 1.06mm.

The predicted TR is in slight excess of 12:1. The maximum acceleration happens at the location of ~ 8.5 mm behind the drive bunch, and is expected to be 6MV/m for a 50nC drive bunch. The drive bunch excites several modes (LSM and LSE), mainly

pumping energy into LM₃₁, LE₁₁, LM₂₁ and LM₁₁, presented here in a descending order as to the amount of power they receive. The LM₃₁-mode frequency is ~30GHz.

The module was tested at Argonne Wakefield Accelerator facility (AWA). The experimental layout is given by Fig.2.

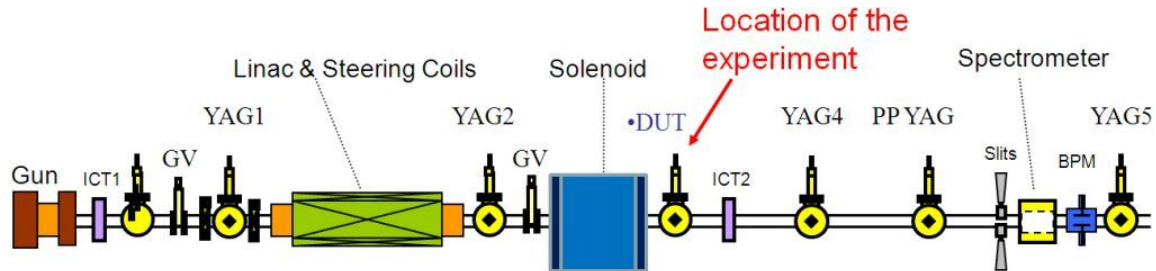


Fig.2: Experimental layout.

Both the drive and the test bunch are produced at the same RF photocathode and accelerated to ~14MeV in the same rf LINAC. The drive bunch is produced on the axis of the cathode; its trajectory almost coincides with the beam-line axis with which the apparatus drive channel is aligned [that is, the middle of the drive channel is put on the beam-line axis]. The test bunch is produced off-axis so that it may enter the test channel which is located off-axis of the beam-line. The position and focusing of the test bunch are determined by the same controls that focus and guide the drive bunch [16].

Fig.3 presents some photos.

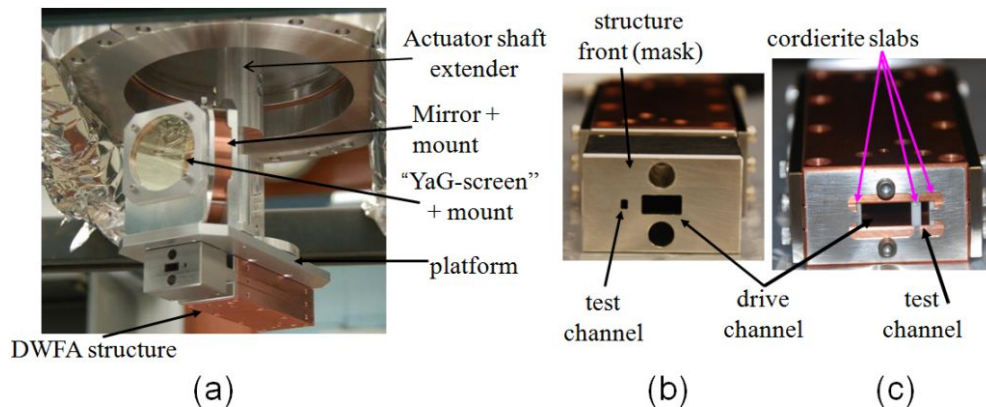


Fig.3: a) DWFA apparatus attached to an actuator before it is placed in the vacuum chamber; (b) front view (the apparatus is preceded by a mask to protect the dielectric slabs from the beam halo); and (c) back view of the accelerator structure.

It is recognized that two-channel rectangular structures of small height are prone to bunch instability and will cause a bunch deflection due to intrinsic asymmetry. Our analysis has shown that the structure length should not exceed 10 cm for the test bunch to clear the test channel without hitting the walls. The maximum deflection is caused in the horizontal plane by a relatively large F_x -force of ~ 0.8 MV/m [if the 50nC drive is used], but the F_y -force is small and does not contribute much to test bunch deflection. We emphasize that these limitations do not prevent us from studying the basic physics. Also, we point out that the device may find application as a fast “kicker” [17].

II. Numerical Simulations

Table I shows the design parameters of the two-channel dielectric-lined wakefield accelerator module, as provided by numerical studies [16 & 18] using the CST Studio Code.

Table I: parameters of the two-channel dielectric-lined wakefield accelerator module.

LSM ₃₁ design mode eigenfrequency (for $v_{\text{phase}} = c$)	30 GHz
Drive channel dimensions	12 x 6 mm
Accelerating channel dimensions	2 x 6 mm
Transformer ratio	12.6 : 1
Dielectric [cordierite] slab #1 thickness	1.24 – 1.25 mm
Dielectric [cordierite] slab #2 thickness	2.29 -2.3 mm
Dielectric [cordierite] slab #3 thickness	1.05 – 1.06 mm
Dielectric relative constant	4.76
Drive bunch size, $\sigma_x \times \sigma_y \times \sigma_z$	3 x 1 x 2 mm
Bunch energy entering apparatus	~14 MeV
Drive bunch charge	10 - 50 nC
Number of drive bunches	1

Table II shows the amount of power going into the eigenmodes if the module is excited by a 50nC drive bunch. As already stated, LM₃₁, LE₁₁, LM₂₁ and LM₁₁ are the modes into which the bunch radiates most of its power. Fig 4. a presents some of the modes [normalized similarly].

Table II: Eigen frequencies of two-channel structure and radiation power for the Gaussian distribution of charge within the 50nC drive bunch

Mode	Frequency, GHz	Power, MW	Mode	Frequency, GHz	Power, MW
LSM ₁₁	24.79	0.52	LSE ₁₁	19.96	2.5
LSM ₂₁	29.97	1.07	LSE ₂₁	39.07	0.135
LSM ₃₁	30.00	2.41	LSE ₃₁	44.68	$9.6 \cdot 10^{-2}$
LSM ₄₁	53.61	$4.36 \cdot 10^{-2}$	LSE ₄₁	45.40	0.26
LSM ₅₁	75.42	$8.36 \cdot 10^{-5}$	LSE ₅₁	72.99	$1.94 \cdot 10^{-4}$

The wakefield being a superposition of LSM and LSE mode wave functions, the composite accelerating force F_z is shown in Fig.4.b; Fig.5.a presents the map of the composite axial force F_z as a function of x and z in the plane $y = 0$.

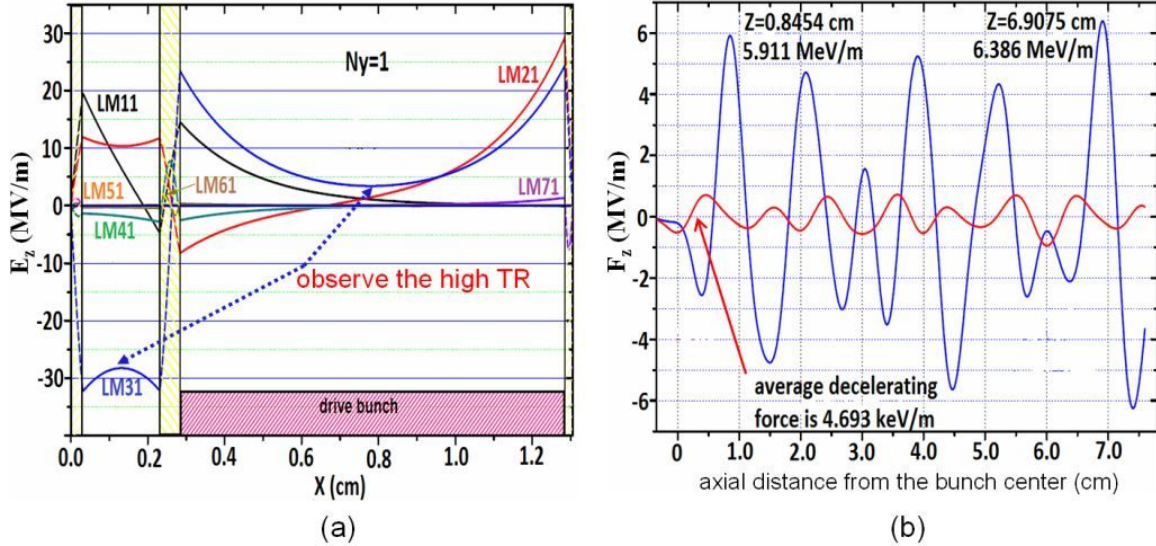


Fig.4: (a) Some of the modes which may be excited by a drive bunch. The modes shown are normalized similarly. However, an analysis has shown that the drive bunch will excite mostly LM_{31} , LE_{11} , LM_{21} and LM_{11} modes. The resulting wakefield will impose a composite F_z -force on the test bunch as shown in (b). These curves are given for a 50nC drive bunch. The curve with the large magnitude is the accelerating force acting on the test bunch, and the curve with the small magnitude is the decelerating force acting on the drive bunch (at the center of the drive channel). The vertical scale is (1 MV/m)/div, and the horizontal scale is (1 cm)/div.

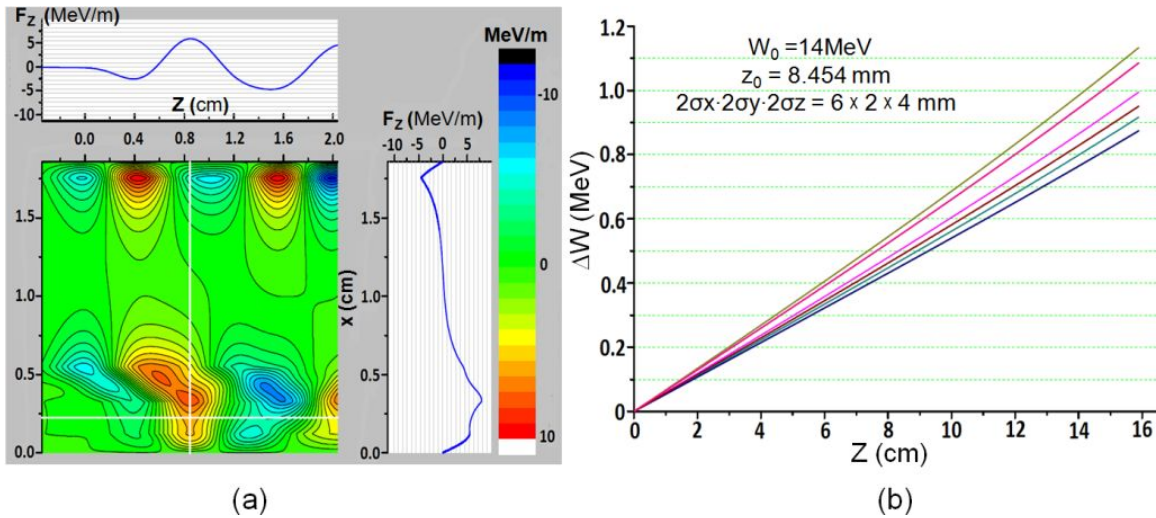


Fig.5: (a) The composite axial force $F_z(z, x)$ in the plane $y = 0$. The middle of test bunch is at the white cross-hair [CST Studio simulations at Kharkov Institute]; (b) A monoenergetic test bunch with rms-length ~ 2 mm will experience about 6% energy spread after traveling 10 cm, obtained from the analysis of different trajectories [see comments in the text]. Here the vertical scale is 0.1 MeV/div; the horizontal scale is 1cm/div.

Depending on the relative delay between the drive and test bunches, the length of the test bunch, and the drive bunch charge, the test bunch may either acquire an additional energy

spread, or have its energy spread reduced. The particular details will be given later, when we present analysis of the experimental data and comparison with the model predictions.

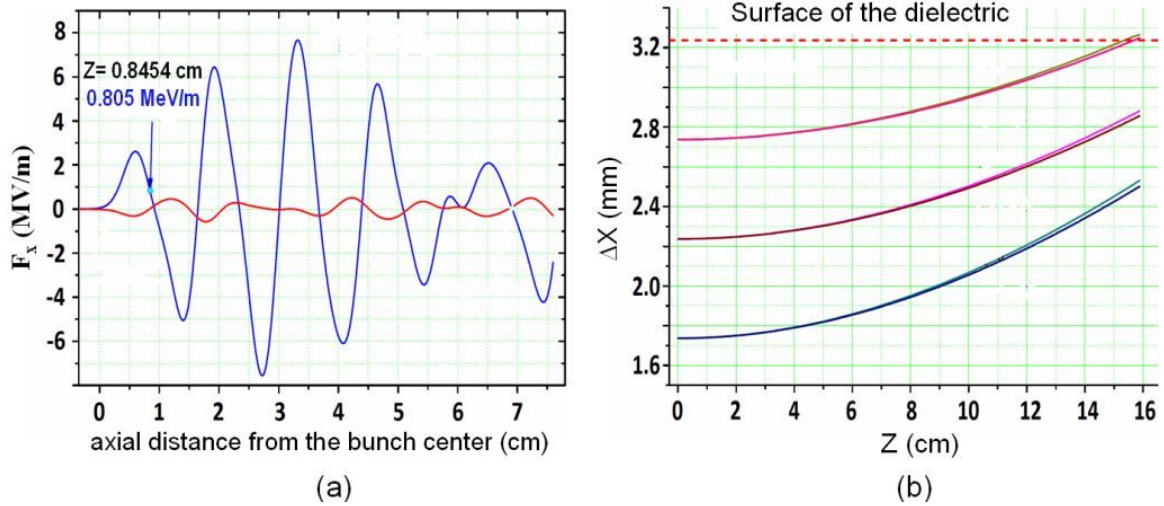


Fig.6: (a) Axial profile of the composite horizontal force F_x ($y = 0$) along the center of the acceleration channel (blue curve) and the center of the drive channel (red); and (b) the X-position of test particles as they move along the structure. The initial energy is taken to be 14 MeV. A few test particles are tracked in the wakefield set up by a 50nC drive bunch, each test particle having its initial axial position $z = 0.8454$ cm, which corresponds [see Fig.4] to the maximum of accelerating force F_z .

The deflecting forces in the horizontal (x-) direction can be large [see Fig.6], however, they still permit test bunch transmission without interception along the 10cm long module. The net deflecting forces in the vertical (y-) direction are nearly absent in the vicinity of the center of test channel; the nature of vertical forces, F_y , is either focusing or defocusing depending on the test bunch location. However [see Fig.7] the influence of the vertical forces on the bunch dynamics is substantially less than the horizontal forces.

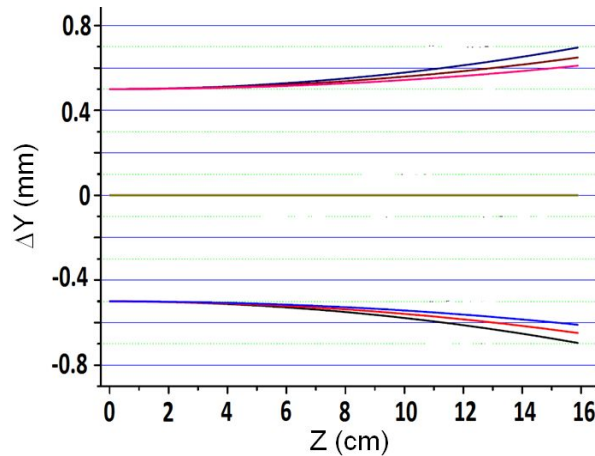


Fig.7: the Y-position of test particles as they move along the structure. The initial energy is taken to be 14 MeV. A few test particles are tracked in the wakefield set up by a 50nC

drive bunch, each test particle having its initial axial position $z = 0.8454\text{cm}$, which corresponds [see Fig.4] to the maximum of the accelerating force F_z .

Given the results listed above, the length of module for this proof-of-principle experiment was chosen to be 10cm.

III. Design Details and Bunch Transport Matters

Critical aspects of the apparatus included means for precise assembly of the rectangular two-channel DWFA module. Fig. 8 shows how all three cordierite slabs are positioned with high accuracy in a copper block to form the structure, wherein shallow protrusions capture the slabs.

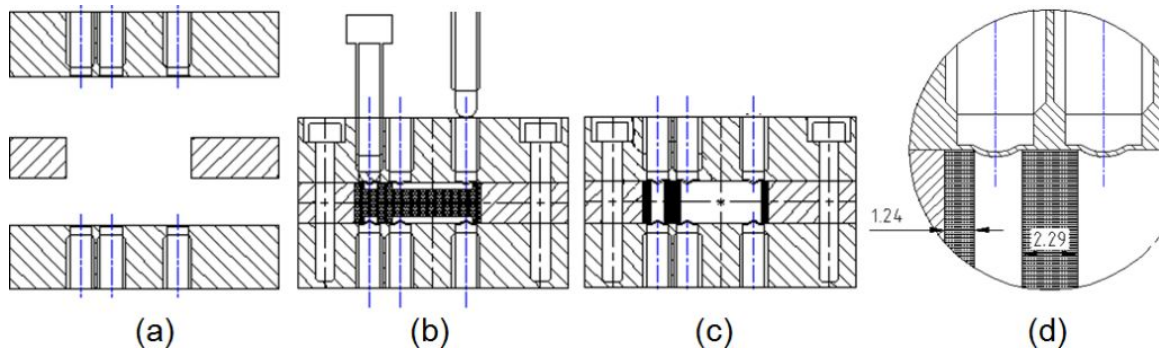
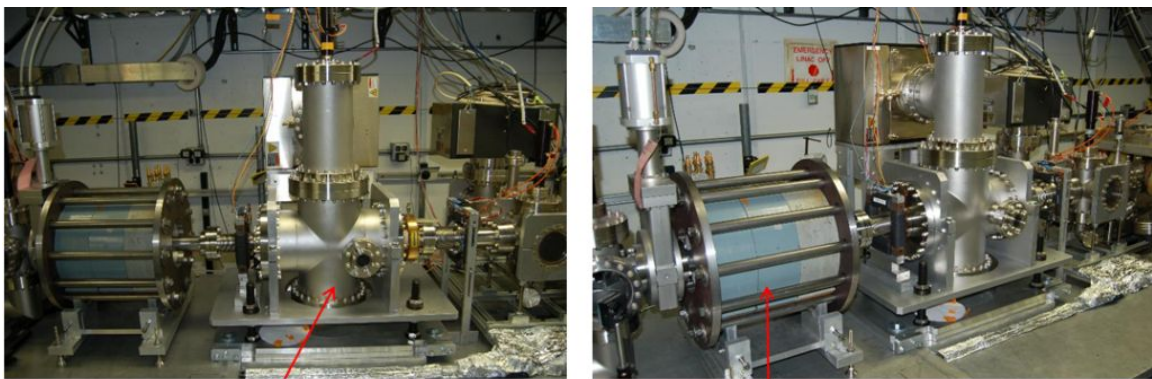


Fig.8: In order to position the dielectric slabs with high accuracy, (a) at a few locations along its length the structure has triplets of holes the depth of which ensures that a thin wall is formed between the bottom of each hole and the inner volume of the apparatus. (b) A steel form is inserted, whose protrusions reproduce precisely the slabs dimensions, and are located as far as the slabs should be. The pushing screws (top) are used to produce another set of protrusions in the copper blocks, each facing inward, as shown in (d), so as to capture the dielectric slabs when inserted as shown in (c).



Chamber for apparatus

Solenoid [$\sim 20\text{ Gs/ Amp}$; 32 cm long]

Fig.9: Chamber for housing and positioning the DWFA module on the AWA beam-line

Fig.9 shows the vacuum chamber in which the DWFA structure is supported, with an actuator for positioning it on the beam axis and with a beam imaging target that can be

interposed for alignment. The final focusing of the drive bunch that propagates along the beam-line axis is done using the 32cm-long solenoid.

A time-delayed test bunch is produced off-axis on the same photocathode where the drive bunch was produced. The test bunch is made by a second laser pulse that is formed by diversion off a splitter from the main pulse used to create the drive bunch. The test bunch propagates off-axis, and its position and focusing is determined by the same controls (LINAC, magnets) that guide and focus the drive bunch. Simulations indicated that a test bunch can be delivered to the required location while the drive bunch is still focused and positioned as desired [Fig.10]; however, each time the gun phase or delay between the bunches is adjusted, a careful optimization is required to have both bunches transmitted through the apparatus.

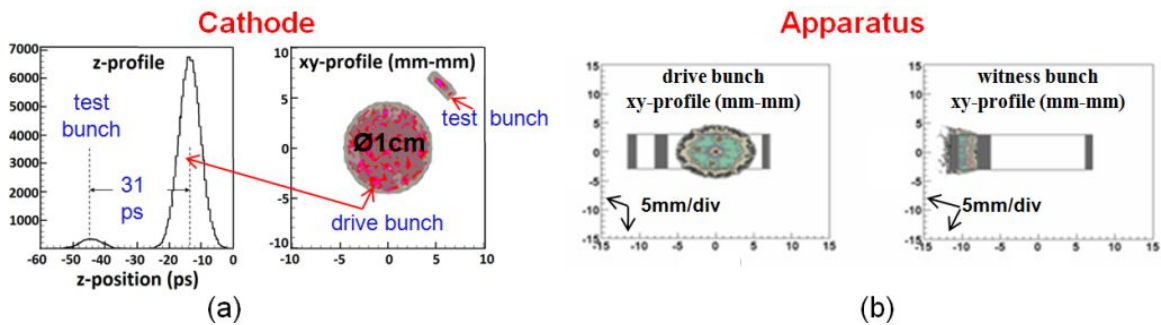


Fig.10: Simulations indicate that both bunches produced at the cathode (a) can be guided and focused to the correct locations when delivered to the apparatus (b). The simulation is done for 10^5 particles (the left graph in (a) shows the number of particles vs. initial z-coordinate for both bunches).

Given the narrow size of the test channel preceded by a mask to collimate the beams, the transmission of the test bunch requires both accurate positioning and having a correct angle. Under these circumstances it was found that the test bunch can be transmitted only when the solenoid does not deliver too strong focusing. This, in turn, did not allow us to use drive bunches with drive charges exceeding 15nC; otherwise the under-focused drive bunch would partially leak into the test channel and prevent imaging of the test bunch on the spectrometer screen.

Another complicating factor is that the horizontal separation between bunches was measured to be typically 7mm. Given that the spacing between the centers of the two channels is 9.6mm, the drive bunch was typically located away from [schematic in Fig.11] the drive channel center axis by 2-3 mm. These practical difficulties indicate that two-bunch schemes are better tested if a facility is equipped with two guns, and two separate beam lines to produce and manipulate the beams independently.

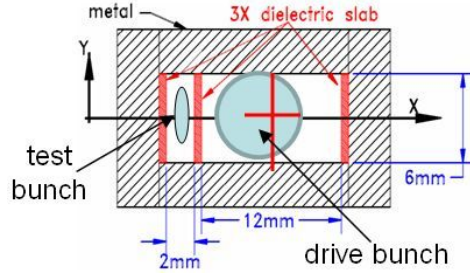


Fig.11: Horizontal separation between bunches was measured to be typically 7mm, whereas the spacing between the centers of channels is 9.6mm. This means that the drive bunch needed to be located off the drive channel center by 2-3 mm.

IV. Experimental Results vs. Model Predictions: Changes in Bunch Energy after Acceleration

Data were collected for three different delays between the drive bunch and the test bunch, namely ~6mm, ~11mm, and ~22 mm. For each delay multiple shots were recorded on the spectrometer screen; the typical information is the energy gain/ loss received by electrons and the horizontal deflection (kick) received by electrons; the first one is read by taking vertical projections of the image on the screen, the second one is read by taking horizontal projections on the screen [16 & 18]. The energy slit helps to narrow the energy value; being positioned horizontally, the energy slit, however, does not affect the readouts to infer the horizontal deflection of the bunch, which is later processed to obtain the value of the responsible horizontal deflecting force [17].

To study the changes in energy distribution caused by the interaction between the test bunch and the wakefields set up by the preceding drive bunch, the method described in Appendix A.I is used.

With the delay ~6 mm [see Fig.12.b], the typical energy loss was up to 50 – 100keV and the energy gain was up to 90 - 100keV; on average the energy changed by ~0keV. Fig.12.a shows that with the delay ~6mm, to have the observed energy loss the accelerating force F_z (re-computed for 50nC of the drive charge) must be up to -4.95/ - 5.5MeV/m; to have the observed gain, F_z must be up to +2.75 / 5.5 MeV/m. All these values (pointed at by the red arrows) can be found on the $F_z(z)$ curves when the drive bunch is x-shifted from the apparatus center by 2-3mm as observed in the experiment.

A very good agreement is seen between the theory model predictions [Fig 12.c] and the observed data [Fig 12. b].

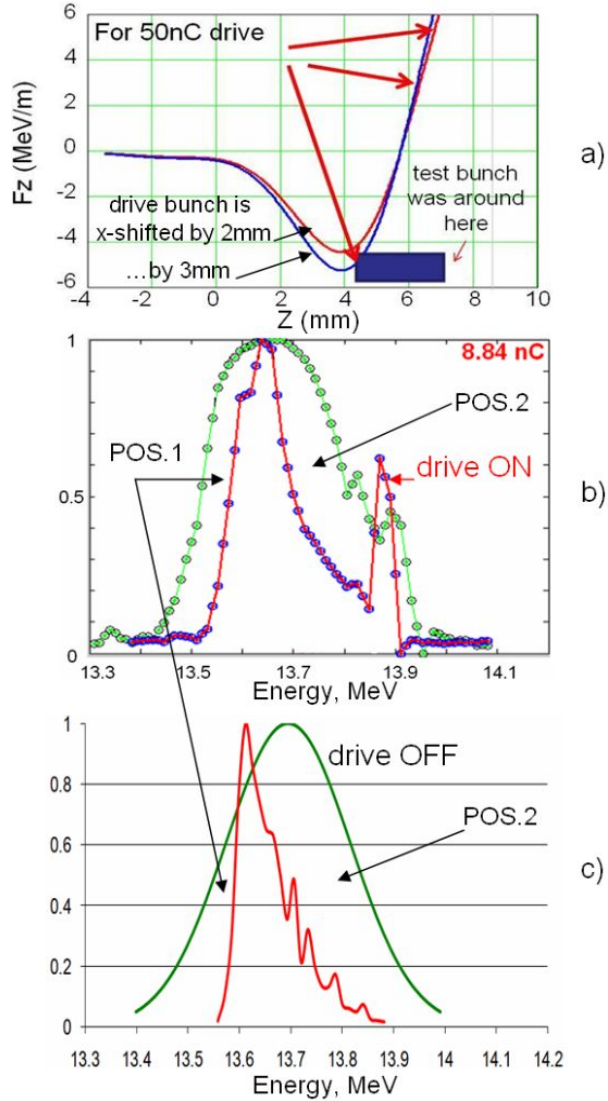


Fig. 12: When the delay was 5.7mm a typical energy distribution observed in 80-85% of shots and normalized to 1 is shown in (b). Simulations of F_z by CST Microwave Studio for the test channel suggest that the test bunch was exposed to F_z ranging from -0.1 to +0.11 MeV/m per nC of the drive charge. All these values (re-normalized here to a 50nC of drive charge) can be found as shown in (a) at the location where the test bunch was during its acceleration in the DWFA module. (c) presents simulations to predict changes in the energy distribution [for case #1 in Table A.I, and the drive bunch is shifted off the center of its channel by 2mm (toward the test channel)]. The slope of final energy distribution (drive ON) in pos.1 is sharper than the slope in pos.2 in both experiment and simulations. Also, the final energy distribution – in both experiment and simulations – shrinks inward of the initial energy distribution (drive OFF).

For delay ~ 11 mm [Fig.13.b], the jitter of 50-60keV; and the energy slit error 77keV required some corrections. Taking these into account, the energy loss was up to 65keV, while the energy gain was in the range 65 - 150keV; the average energy change

was $\sim 50\text{keV}$. When the aforementioned values are re-calculated to 50nC of the drive charge and normalized per 1m , an excellent agreement can be found between the theory and measurements. To have loss, F_z (re-computed for a 50nC drive bunch) must be up to -2.85 MeV/m ; to have observed gains, F_z must be between $+2.85 / 6.7\text{ MeV/m}$. All these values (pointed at by the red arrows) can be found on the $F_z(z)$ curves just exactly where the test bunch was [Fig 13.a].

A very good agreement is seen between the theory model predictions [Fig 13.c] and the observed data [Fig 13. b], when one looks at the changes in energy distribution caused by the interaction between the test bunch and the wakefields.

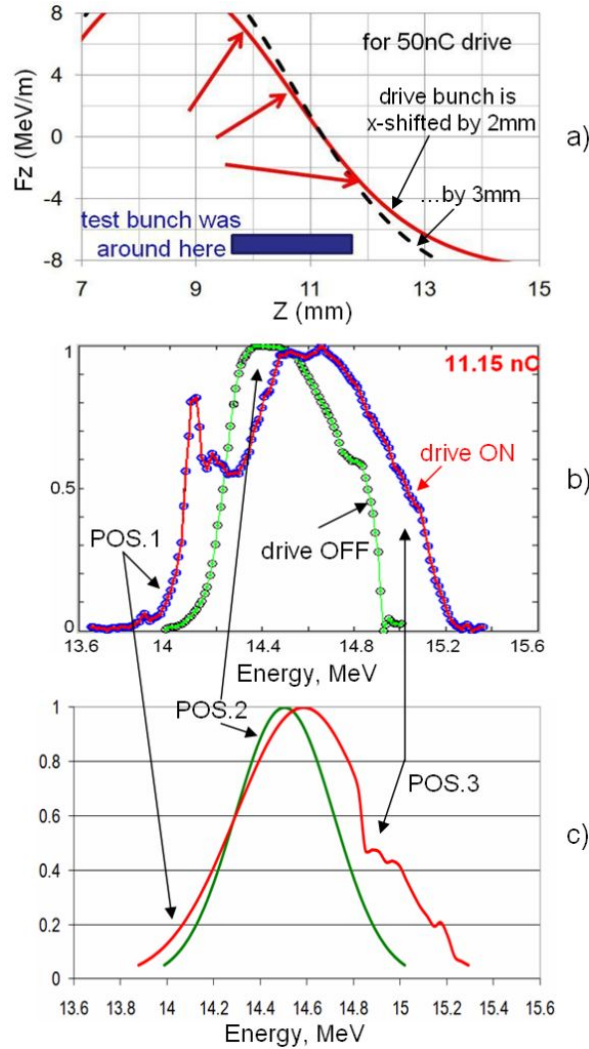


Fig.13: (b) shows a typical energy distribution (observed in 80% of shots) when the delay was 10.7mm (distribution is normalized to 1). Simulations of F_z by CST Microwave Studio for the test channel suggest that the test bunch was exposed F_z ranging from -0.06 to 0.135 MeV/m per every nC of the drive charge. All these values (re-normalized here to a 50nC of drive charge) can be found as shown in (a) at the location where the test bunch was during its acceleration in the DWFA module. (c) shows simulations to predict changes in the energy distribution [for case #2 in Table A.I, and the drive bunch being

shifted off the center of its respective channel by 2mm (toward the test channel)]. Here in pos.1 the final energy distribution (drive ON) moves to the left in both top and bottom figures as compared to the initial distribution (drive OFF). In pos.2 the final energy distribution moves “inward” of the initial one, again on both plots. In pos. 3, the behavior is again the same.

For delay $\sim 22\text{mm}$ [Fig.14.b], the jitter of 40-50keV and the energy slit error 77-154keV required some corrections. The energy gain was up to 350keV; the average energy change was $\sim 170\text{-}220\text{keV}$. When the aforementioned values are re-calculated to 50nC of the drive charge and normalized per 1m, an excellent agreement can be found between the theory and measurements. To have observed gains, F_z must be up to +9 MeV/m, but on average 6.5 – 8.5MeV/m. Again F_z are re-computed for a 50nC drive bunch, and all the values are found on the the $F_z(z)$ curves exactly where the test bunch was [see Fig 14.a].

As in the former cases, a very good agreement is seen between the theory model predictions [Fig 14.c] and the observed data [Fig 14. b], when one looks at the changes in energy distribution caused by the interaction between the test bunch and the wakefields.

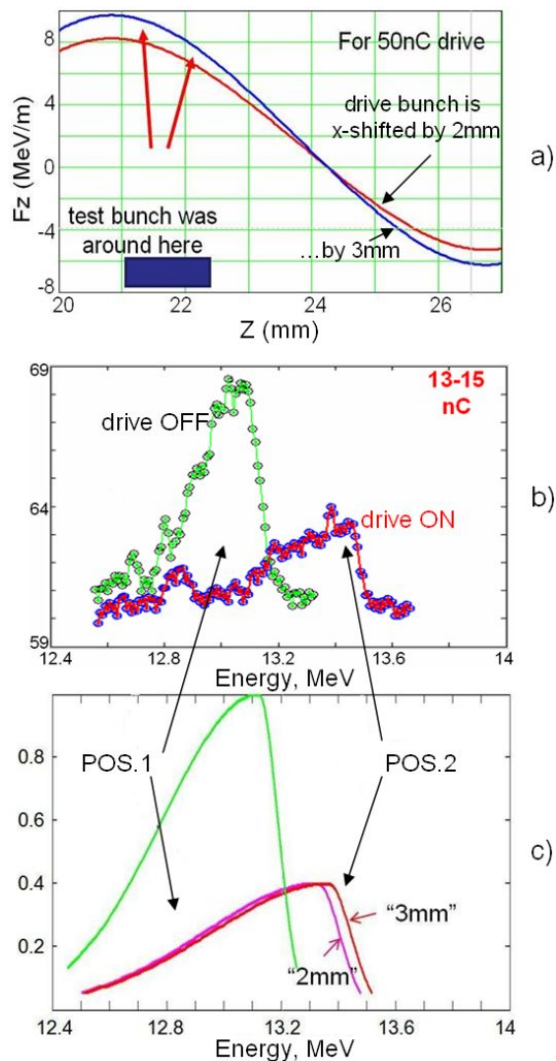


Fig.14: Typical energy distribution (observed in 80% of shots) when the delay was 21.7mm is shown in (a); note that these are examples of non-normalized distributions. Simulations of F_z by CST Microwave Studio for the test channel suggest that the test bunch was exposed to F_z ranging from 0.13 to 0.18 MeV/m per each nC of the drive charge. All these values (re-normalized here to a 50nC of drive charge) can be found as shown in (a) at the location where the test bunch was during its acceleration in the DWFA module. (c) shows simulations to predict changes in the energy distribution (for case #3 in Table A.I). The final distribution (drive ON) is shown when the drive bunch is shifted off the center of its respective channel by 2mm and 3mm (curves are pointed at by “2mm” and “3mm” respectively in the bottom plot). In pos.1 and pos. 2, the evolution of final energy distribution is the same in both top and bottom figures as compared to the initial distribution (drive OFF). Note that some particle losses do occur in this case.

V. Changes in Bunch Horizontal Distribution after Acceleration: Experimental Results vs. Model Predictions

Here again, the data were collected for the same three different delays between the drive bunch and the test bunch, namely ~6mm, ~11mm, and ~22 mm. For each delay multiple shots were recorded on the spectrometer screen; the horizontal deflection (kick) received by electrons is read by taking horizontal projections on the screen [16]. The energy slit helps to narrow the energy value; being positioned horizontally, the energy slit does not affect the readouts to infer the horizontal deflection of the bunch, which is later processed to obtain the value of the responsible horizontal deflecting force [17].

To study the changes in horizontal distribution (and x-kicks) caused by the interaction between the test bunch and the wakefields set up by the preceding drive bunch, the method described in Appendix A.II is used.

With the delay ~6 mm [see Fig.15. b], the horizontal kick that led to the shift as shown was about 6.18 – 6.8 mrad. When the aforementioned values are re-calculated to 50nC of the drive charge and normalized per 1m, an excellent agreement can be found between the theory and measurements. Fig.15.a shows that to have the measured horizontal kicks the horizontal deflection force F_x (re-computed for 50nC of the drive charge) must be about 4.65 / 5.12 MeV/m. All these values (pointed at by the black arrows) can be found on the $F_x(z)$ curves when the drive bunch is initially x-shifted from the apparatus centre by 2-3mm as observed in the experiment.

A very good agreement is seen between the theory model predictions [Fig 15.c] and the observed data [Fig 15. b], when one looks at the changes in the horizontal distribution caused by the interaction between the test bunch and the wakefields.

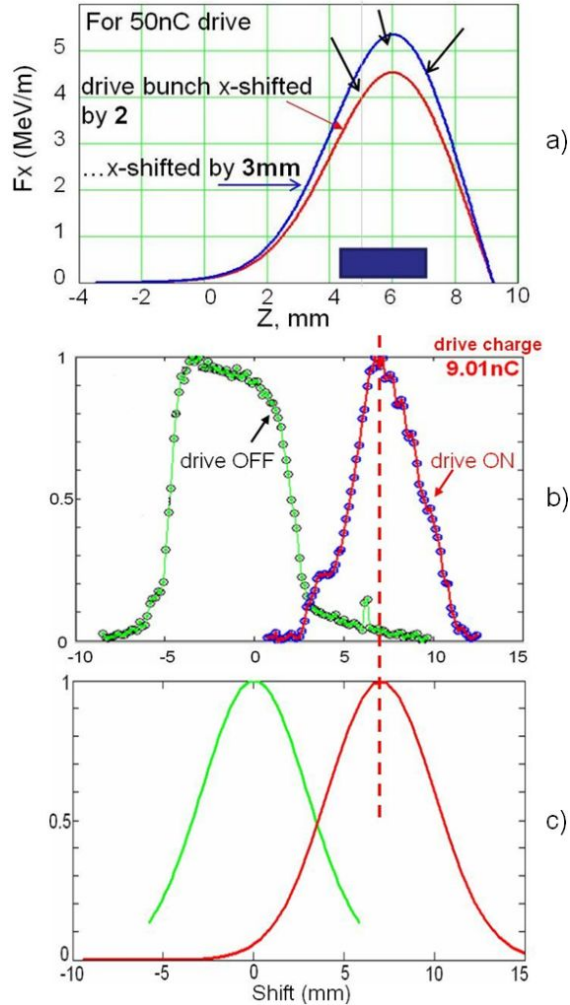


Fig.15: Typical bunch horizontal distribution (observed in 80-85% of shots, normalized to 1) is shown in (b) when the delay was 5.7mm. (a) shows simulations of F_x by CST Microwave Studio for the test channel; the observed X-kick suggests that the test bunch was exposed to F_x ranging from 0.09 to 0.1 MeV/m per nC of the drive charge; all these values (re-normalized here to a 50nC of drive charge) can be found as shown at the location where the test bunch was during its acceleration in the DWFA module. (c) shows simulations that predict changes in the horizontal distribution [for case #1 in Tables A.I and A.II, for the drive bunch being shifted off the center of its respective channel by 2mm (toward the test channel)]. The initial model distribution [drive OFF] has the same FWHM as the experimental one. Observe the same amount of average x-kick for the accelerated test bunch [curves marked by “drive ON”]

For delay ~ 11 mm [Fig.16.b], the horizontal kick that led to the typical shifts presented was ranging from -2.45 to -5.2 mrad; in average it was -3.9 mrad. When the aforementioned values are re-calculated to 50nC of the drive charge and normalized per 1m, an excellent agreement can be found between the theory and measurements. To have x-kicks F_x (re-computed for a 50nC drive bunch) must range between -1.72 and -3.6

MeV/m, and be in average -2.8 MeV/m. Again, all these values (pointed at by the back arrows) can be found on the $F_x(z)$ curves exactly where the test bunch was [see Fig. 16.a].

A very good agreement is again seen between the theory model predictions [Fig 16.c] and the observed data [Fig 16. b], when one looks at the changes in the horizontal distribution caused by the interaction between the test bunch and the wakefields.

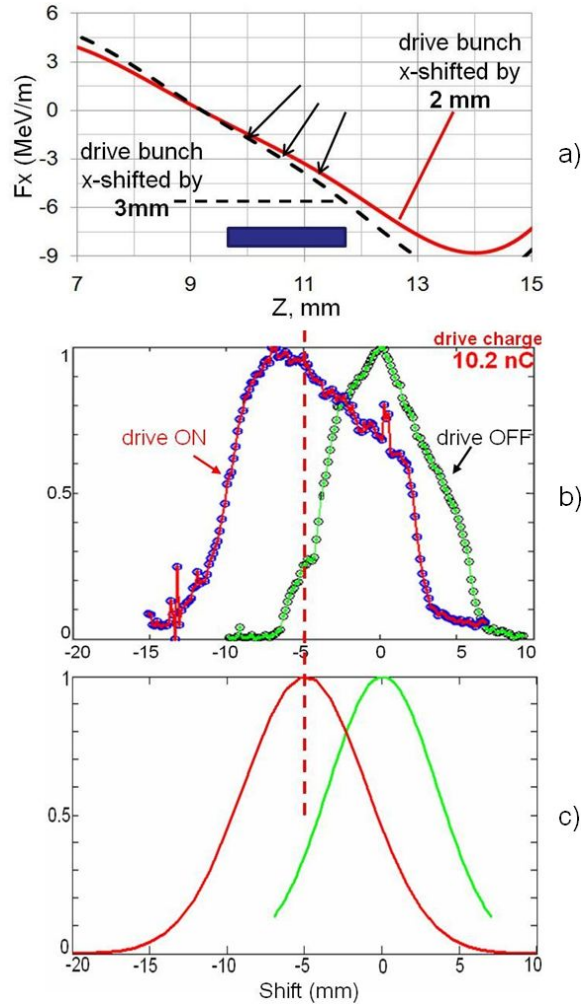


Fig.16: Typical bunch horizontal distribution (observed in 80% of shots, normalized to 1) when the delay was 10.7mm shown in (b). (a) shows simulations of F_x by CST Microwave Studio for the test channel; the observed X-kick suggests that the test bunch was exposed to F_x ranging from -0.034 to -0.072 MeV/m per nC of the drive charge; all these values (re-normalized here to a 50nC of drive charge) can be found as shown at the location where the test bunch was during its acceleration in the DWFA module. (c) shows the predicted changes in horizontal distribution [case #2 in Tables A.I and A.II with the drive bunch being shifted off the center of its respective channel by 2mm (toward the test channel)]. The initial model distribution [drive OFF] has the same half-width as the experimental one. Observe nearly the same amount of average x-kick for the accelerated test bunch [curves marked by “drive ON”]; also in both experiment and theory FWHM appears to remain the same before and after acceleration

For delay $\sim 22\text{mm}$ [Fig.17.b], the horizontal kick was inferred to be about $+12.2$ mrad. When the aforementioned values are re-calculated to 50nC of the drive charge and normalized per 1m , an excellent agreement can be found between the theory and measurements [see Fig. 17. a]. To have the resulting x-kicks F_x must be about $5.4\text{-}6.1$ MeV/m. Again, F_x are re-computed for a 50nC drive bunch, and all the values are found on the $F_x(z)$ curves exactly where the test bunch was.

As in the former cases, a very good agreement is again seen between the theory model predictions [Fig 17.c] and the observed data [Fig 17. b], when one looks at the changes in the horizontal distribution caused by the interaction between the test bunch and the wakefields.

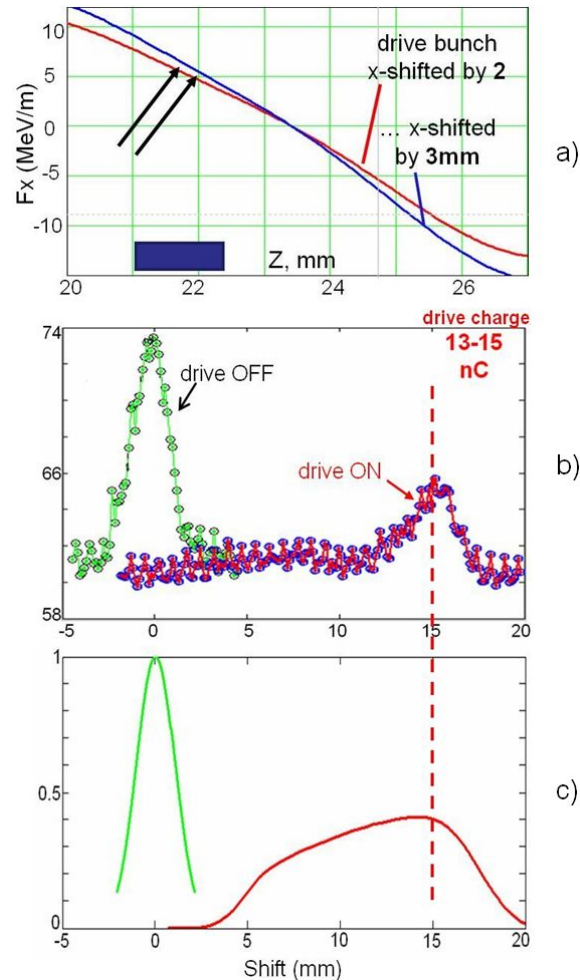


Fig. 17: (b) Typical bunch horizontal distribution (observed in 80% of shots) when the delay was 21.7mm ; note that these are examples of non-normalized distributions. (a) shows simulations of F_x by CST Microwave Studio for the test channel; the observed X-kick suggests that the test bunch was exposed to F_x ranging from 0.11 to 0.122 MeV/m per nC of the drive charge; all these values (re-normalized here to a 50nC of drive charge) can be found as shown at the location where the test bunch was during its acceleration in the DWFA module. (c) shows simulations to predict the changes in horizontal distribution [for case #3 in Tables A.I and A.II with the drive bunch being shifted off the center of its respective channel by 2mm (toward the test channel)]. The initial model distribution [drive OFF] has the same half-width as the experimental one.

Observe nearly the same amount of x-kick for the accelerated test bunch [curves marked by “drive ON”] where the distribution has its peak; also in both experiment and theory, the left slope is far more elongated than the right slope in the final distribution

VI. Conclusions

To the best of our knowledge, the experiments just described are the first in which a two-channel, dielectric-lined, rectangular, wakefield structure has been tested. It is found that the experimental data are very well explained by the theory model predictions. The theory model includes the wakefield simulations using the CST Studio together with reasonable assumptions regarding the input distribution of bunch particle energies and positions.

Of course, introducing a narrower test bunch at particular values of the delay would secure both high acceleration and low deflection. Nevertheless, the presence of deflection in a rectangular DWFA is an intrinsic feature [17] that is a consequence of its lack of symmetry. An exceedingly better choice for accelerator application may be a coaxial structure where symmetry cures this unwanted deflection [12 & 15]. The rectangular version – studied [14, 16-18] and developed [14 & 16] by our group – nonetheless delivers a useful example that is very well suited to check theory and our understanding of how the device operates.

Finally, we note that the aforementioned practical difficulties to operate a two-bunch scheme as described in section II, where both bunches are produced at the same RF photocathode with one of them delayed and propagating off the beam-line axis, recommend strongly that two-bunch schemes are better tested at a facility that is equipped with two guns to produce, and two separate beam-lines to manipulate, the bunches independently.

Acknowledgments

The authors would like to acknowledge the financial support of U.S. Department of Energy (Office of High Energy Physics), and also express many thanks to A. Didenko (former Omega-P contractor) for his excellent mechanical design for the rectangular DWFA module and related hardware, and to J. Zmuda, M. Lien, and R. Konecny (Argonne National Lab.) for their help during the installations, operation, and especially for refurbishing the modulator that enabled us to have excellent operational stability--much needed for this experiment which required two time-delayed bunches that originate at the same photocathode with the second one produced and delivered off the beam-line axis.

References

1. “Improved ramped bunch train to increase the transformer ratio of a two-channel multimode dielectric wakefield accelerator”, G. V. Sotnikov, and T. C. Marshall, Phys. Rev. ST Accel. Beams **14**, 031302 (2011)

2. "The Dielectric Wakefield Accelerating Structure", A. Kanareykin, S.P. Antipov, J.B. Butler, C.-J. Jing, P. Schoessow, W. Gai, Proc. of 2011 Particle Accelerator Conf. New York, NY, USA, March 28-April 1, 2011, p. 319, eds. T. Satotaga and K. Brown (BNL)
3. "High Frequency High Gradient Dielectric Wakefield Acceleration Experiment at SLAC and BNL", J. Rosenzweig, et al., AIP Conf. Proc. 1299, 364 (2010), eds. S.H. Gold and G.S. Nusinovich, and refs. Therein
4. "Field analysis of a dielectric-loaded rectangular waveguide accelerating structure", Liling Xiao, Wei Gai, and Xiang Sun, Phys. Rev. **E 65**, 016505 (2001)
5. "Wakefield excitation in multimode structures by a train of electron bunches", J. G. Power, Wei Gai, and Paul Schoessow, Phys. Rev. **E 60**, 6061 (1999)
6. "Measurements of the longitudinal wakefields in a multimode, dielectric wakefield accelerator driven by a train of electron bunches", J. G. Power, M. E. Conde, W. Gai, R. Konecny, P. Schoessow, and A. D. Kanareykin, Phys. Rev. ST Accel. Beams **3**, 101302 (2000)
7. "Numerical simulations of intense charged-particle beam propagation in a dielectric wake-field accelerator", W. Gai, A. D. Kanareykin, A. L. Kustov, and J. Simpson, Phys. Rev. **E 55**, 3481 (1997)
8. "Experimental Demonstration of Wakefield Acceleration in a Tunable Dielectric Loaded Accelerating Structure", C. Jing, A. Kanareykin, J. G. Power, M. Conde, W. Liu, S. Antipov, P. Schoessow, and W. Gai, Phys. Rev. Lett. **106**, 164802 (2011)
9. "Increasing the transformer ratio at the Argonne wakefield accelerator", C. Jing, J. G. Power, M. Conde, W. Liu, Z. Yusof, A. Kanareykin, and W. Gai, Phys. Rev. ST Accel. Beams **14**, 021302 (2011)
10. Recent Experiments on Wakefield Transformer Ratio Enhancement at AWA", C. Jing, et al., "AIP Conf. Proc. 1299, 348 (2010), eds. S.H. Gold and G.S. Nusinovich
11. "Development of a Ferroelectric Based Tunable DLA Structure", A. Kanareykin, et al., AIP Conf. Proc. 1086, 386 (2009), eds. C.B Schroeder, W. Leemans and E. Esarey.
12. "A THz Coaxial Two-Channel Dielectric Wakefield Structure for High Gradient Acceleration", T. C. Marshall, G. V. Sotnikov, and J. L. Hirshfield, AIP Conf. Proc. 1299, 336 (2010), eds. S.H. Gold and G.S. Nusinovich
13. "Accelerated Bunch Stability in a Coaxial Dielectric Wakefield Structure When its Symmetry is Broken" G. V. Sotnikov, T. C. Marshall, J. L. Hirshfield, and S. V. Shchelkunov, AIP Conf. Proc. 1299, 342 (2010), eds. S.H. Gold and G.S. Nusinovich
14. "Analysis of a Symmetric Terahertz Dielectric-Lined Rectangular Structure for High Gradient Acceleration", T. C. Marshall, G. V. Sotnikov, S. V. Shchelkunov, and J. L. Hirshfield, AIP Conf. Proc. 1086, 421 (2009), eds. C.B Schroeder, W. Leemans and E. Esarey.
15. "Coaxial two-channel high-gradient dielectric wakefield accelerator", G. V. Sotnikov, T. C. Marshall, and J. L. Hirshfield, Phys. Rev. ST Accel. Beams **12**, 061302 (2009)
16. "Status of Dielectric-Lined Two-Channel Rectangular High Transformer Ratio Accelerator Structure Experiment" S.V. Shchelkunov, M.A. LaPointe, M.E. Conde, W. Gai, J.G. Power, Z.M. Yusof, J.L. Hirshfield, T.C. Marshall, D. Mihalcea, G.V. Sotnikov, Proc. of 2011 Particle Accelerator Conf. New York, NY, USA, March 28-April 1, 2011, p. 298 link: <http://www.cad.bnl.gov/pac2011/proceedings/papers/mop107.pdf>, eds. T. Satotaga and K. Brown (BNL) and refs therein.
17. "A Fast Kicker Using a Rectangular Dielectric Wakefield Accelerator Structure", J.L. Hirshfield, T.C. Marshall, S.V. Shchelkunov, G.V. Sotnikov, Proc. of 23rd Particle Accelerator Conf. (PAC2009), Vancouver, BC, Canada, May 4-8, 2009, p. 4267, ed. M. Comyn (TRIUMF)
18. "Two-Channel Rectangular Dielectric Wake Field Accelerator Structure Experiment", G. V. Sotnikov, T. C. Marshall, S. V. Shchelkunov, A. Didenko, and J. L. Hirshfield, AIP Conf. Proc. 1086, 415 (2009), eds. C.B Schroeder, W. Leemans and E. Esarey.
19. "Experimental observation of constructive superposition of wakefields generated by electron bunches in a dielectric-lined waveguide", S. V. Shchelkunov, T. C. Marshall, J. L. Hirshfield, M. A. Babzien, and M. A. LaPointe, Phys. Rev. ST Accel. Beams **9**, 011301 (2006)
20. "Observation of Superposition of Wake Fields Generated by Electron Bunches in a Dielectric-Lined Waveguide", S. V. Shchelkunov, T. C. Marshall, J. L. Hirshfield, M. A. Babzien, and M. A. LaPointe, Proc. of the 2005 Particle Accelerator Conf, p.3609, (2005), ed. C. Horak (ORNL/SNS)
21. "Wakefield generation by a relativistic ring beam in a coaxial two-channel dielectric loaded structure", Wanming Liu and Wei Gai, Phys. Rev. ST Accel. Beams **12**, 051301 (2009)

22. “Dipole-mode wakefields in dielectric-loaded rectangular waveguide accelerating structures”, Chunguang Jing, Wanming Liu, Liling Xiao, Wei Gai, P. Schoessow, and Thomas Wong, Phys. Rev. E **68**, 016502 (2003)
23. “Diamond-Based Dielectric Loaded Accelerating Structures”, S. Antipov, et al., AIP Conf. Proc. 1299, 359 (2010), eds. S.H. Gold and G.S. Nusinovich
24. “Development of Transverse Modes Damped DLA Structure”, C. Jing, et al., AIP Conf. Proc. 1086, 433 (2009), eds. C.B Schroeder, W. Leemans and E. Esarey.
25. “Observation of Enhanced Transformer Ratio in Collinear Wakefield Acceleration”, C. Jing, A. Kanareykin, J. G. Power, M. Conde, Z. Yusof, P. Schoessow, and W. Gai, Phys. Rev. Lett. **98**, 144801 (2007)
26. “Upgrade of the Argonne Wakefield Accelerator Facility (AWA) and Commissioning of a New RF Gun for Drive Beam Generation”, M.E. Conde, D.S. Doran, W. Gai, R. Konecny, W. Liu, J.G. Power, Z.M. Yusof, S.P. Antipov, C.-J. Jing, E.E. Wisniewski, Proc. of 2011 Particle Accelerator Conf. New York, NY, USA, March 28-April 1, 2011, p. 115, eds. T. Satotaga and K. Brown (BNL)
27. “Argonne Wakefield Accelerator Facility (AWA) Upgrades and Future Goals”, M. Conde, link: [https://twindico.hep.anl.gov/indico/getFile.py/access?contribId=29&resId=0&materialId=slides&confId=428#256.1.AWA Facility Upgrade](https://twindico.hep.anl.gov/indico/getFile.py/access?contribId=29&resId=0&materialId=slides&confId=428#256.1.AWA%20Facility%20Upgrade)
28. RF and Space Charge Effects in LASER-Driven Electron Guns”, by Kwang-Je Kim, Nuclear Instruments and Methods in Physics Research, A275, pp. 201-218, (1989)
29. Experimental Observation of High-Brightness Microbunching in a Photocathode RF Electron Gun”, by X. J. Wang, X. Qiu, and I. Ben-Zvi, Phys. Rev. E 54, R3121-R3124 (1996)
30. Experimental Characterization of the High-Brightness Electron Photoinjector”, by X.J. Wang, M. Babzien, K. Batchelor, I. Ben-Zvi, R. Malone, I. Pogorelsky, X. Qui, J. Sheehan, J. Skaritka, and T. Srinivasan-Rao, Nuclear Instruments and Methods in Physics Research A375, (1996), 82-86

Appendix A.I: Changes in Bunch Energy after Acceleration

To study the changes in energy distribution caused by the interaction between the test bunch and the wakefields set up by the preceding drive bunch, it is assumed here and further on that the initial longitudinal distribution in the test bunch resembles a Gaussian one, however, with the head possibly different from the tail. In that case, when a bunch with a small charge is produced by an RF photocathode gun, a validated model [28-30] is

$$n_{ini}(z) = n_o \exp\left(-\frac{(z - Z_{test})^2}{2\sigma_{z,head}^2}\right), \text{ if } z \leq Z_{test} \quad (1. a)$$

$$n_{ini}(z) = n_o \exp\left(-\frac{(z - Z_{test})^2}{2\sigma_{z,tail}^2}\right), \text{ if } z > Z_{test} \quad (1. b)$$

where $n_{ini}(z)$ is the initial particle density, z is the initial longitudinal coordinate of the test particle relative to the drive bunch, Z_{test} is the longitudinal position (delay) of the test bunch center relative to the drive bunch, $\sigma_{z,head}$ and $\sigma_{z,tail}$ are the rms-length of the bunch head and its tail, and n_o is an appropriate normalization constant. The values of delay, Z_{test} , and $\sigma_{z,head}$ and $\sigma_{z,tail}$ as either directly measured in experiment or inferred from processing the experimental data are listed in Table A.I. In this convention it is to be noted that the test bunch, the drive bunch, and the wakefields move from right-to-left, toward lesser z -values.

The correlation between the test particle’s initial position and its energy is important to explain the behavior already presented. This information is not available, so

here we must make an assumption about this correlation; we take it to be approximated by a linear function:

$$E_{ini}(z) = E_{test} - (z - Z_{test}) \frac{\sigma_E}{\sigma_z}, \quad \text{with } \sigma_z = 0.5(\sigma_{z,head} + \sigma_{z,tail}) \quad (2)$$

where $E_{ini}(z)$ is the test particle initial energy, E_{test} is an average initial energy of the test bunch known from the experiment, and σ_E is the rms-energy spread of the test bunch (also known from the experimental curves, see e.g. Figs 12-14). E_{test} and σ_E are listed in Table A.I. σ_z is selected to be computed as indicated below.

The particle initial coordinate z in Eq.1 and Eq.2 is a parameter; thus, one can plot $n_{ini}(z)$ vs. $E_{ini}(z)$ and adjust $\sigma_{z,head}$ and $\sigma_{z,tail}$ to accurately model the observed initial energy distribution as seen in Figs 12-14, (b). These values are presented in Table A.I. The fields/forces that dictate the particle dynamics are known from CST Studio simulations [see Fig. 18].

Table A.I

case #	1	2	3
Z_{test} (mm), delay between drive and test bunches	5.7	10.7	21.7
E_{test} (MeV)	13.7	14.5	13.12
$\sigma_{z,head} / \sigma_{z,tail}$ (mm)	0.6 / 0.6	0.6 / 0.6	0.2 / 1.0
σ_E (MeV)	0.12	0.21	0.2

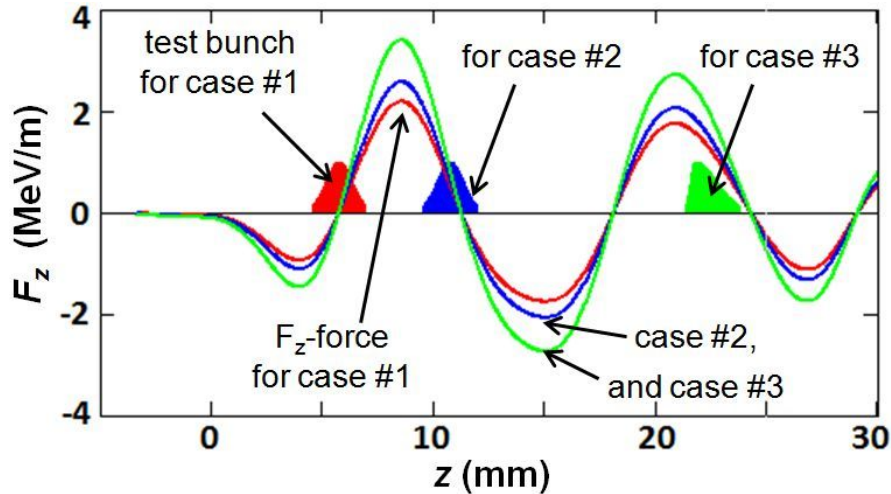


Fig.18: $F_z(z)$ –force acting on the test bunch (traveling behind the drive bunch at locations marked as case 1, or 2 or 3) is shown here computed for 9nC of the drive charge (case #1), 10.6nC of the drive charge (case #2) and 14nC (case #3). The drive bunch is off the center of its respective channel by 3mm toward the test channel. Accordingly, for each case the test bunch position and distribution is different, as indicated.

After the equations of motion are integrated over the apparatus length, L , the final particle position (relative to the drive bunch) and final energy are:

$$z_{fin} = \tilde{Z}(E_{ini}, z) \quad (3. a)$$

$$n_{fin}(z_{fin}) = n_{ini}(z) - PPL \quad (3. b)$$

$$E_{fin} = \tilde{E}(E_{ini}, z) \quad (3. c)$$

where (as before) z is the initial particle coordinate (relative to the drive bunch), E_{ini} is the initial energy, z_{fin} is the final coordinate, $\tilde{Z}(\dots)$ is a function that represents the dependence of z_{fin} on E_{ini} and z , and is obtained after numerical integration; n_{fin} is the particle density at z_{fin} , with PPL representing possible particle losses because some particles may hit the walls of the test channel, E_{fin} is the final energy, and $\tilde{E}(\dots)$ is a function that represents the dependence of E_{fin} on E_{ini} and z , and is also obtained after numerical integration.

Noting that z enters as a parameter in Eq.3, and that Eq.2 provides the correlation between E_{ini} and z , one can mutually exclude z from Eq.3b and c, and then plot n_{fin} vs. E_{fin} to obtain the final energy distribution.

The aforementioned recipes produce results for different delays (~6, ~11, and ~22 mm) as have been presented in Figs 12-14, with a very good agreement seen in all cases.

In particular, in a zero-order approximation, one may assume the absence of particle slippage and transverse motion (because of the short apparatus length, L), and Eq.3 becomes:

$$\begin{aligned} z_{fin} &= z, \\ n_{fin}(z_{fin}) &= n_{ini}(z), \text{ and} \\ E_{fin} &= E_{ini}(z) + F_z(z)L, \end{aligned}$$

where F_z is presented in Fig.18.

In this simplified scenario, the final distribution is, obviously, a plot of

$$n_{ini}(z) \text{ vs. } E_{ini}(z) + F_z(z)L$$

Appendix A.II: Bunch X-Deflection

To study the change in horizontal velocity distribution that results from the transverse wakefield force, we use the following zero-order approximation for the initial test bunch distribution: 1) the bunch is relatively compact horizontally and vertically, that is $\sigma_x = \sigma_y = 0$; 2) the velocity spread in the y-direction is ignored; 3) the velocity spread in the x-direction is taken into account in the particle density distribution function as:

$$N_{ini}(z, \alpha_x) = n_0 n_{ini}(z) \exp\left(-\frac{\alpha_x^2}{2\sigma_{\alpha,x}^2}\right) \quad (4)$$

where $\alpha_x = V_x/c$ is the x-velocity represented as an angular value (rad) with V_x being the horizontal transverse velocity measured in m/sec; $\sigma_{\alpha,x} = \sigma_{v,x}/c$ is the horizontal rms spread represented as an angular value (rad), and c is the speed of light [~ the

longitudinal velocity with which 13-14MeV electrons move]; n_o is an appropriate normalizing constant; $n_{ini}(z)$ is given by Eq.1 in section IV.

Because initially z and α_x have no correlation between each other, the distribution as a function of the x-velocity is simply:

$$N_{ini}(\alpha_x) = n_1 \exp\left(-\frac{\alpha_x^2}{2\sigma_{\alpha,x}^2}\right) \quad (5)$$

where n_1 is an appropriate normalizing constant.

The values of $\sigma_{\alpha,x}$ are found by analyzing the initial horizontal particle distributions available from the experiment. If the distributions are assumed to resemble Gaussian ones, the rms values (mm) seen on the spectrometer screen are merely $1230\text{mm}\cdot\sigma_{\alpha,x}$ because the distance between the apparatus and the screen was/is 1230mm. Practically, it is easier to measure the FWHM, and then cast this to rms-values remembering that $\sigma_{\alpha,x} = \text{FWHM}/2.35$ for any Gaussian distribution. The rms values are listed in table A.II.

Table A.II (see also table A.I)

case #	1	2	3
$1230\text{mm}\cdot\sigma_{\alpha,x}$	2.91 mm	3.5 mm	1.05mm
$\sigma_{\alpha,x}$	2.36 mrad	2.84 mrad	0.85 mrad

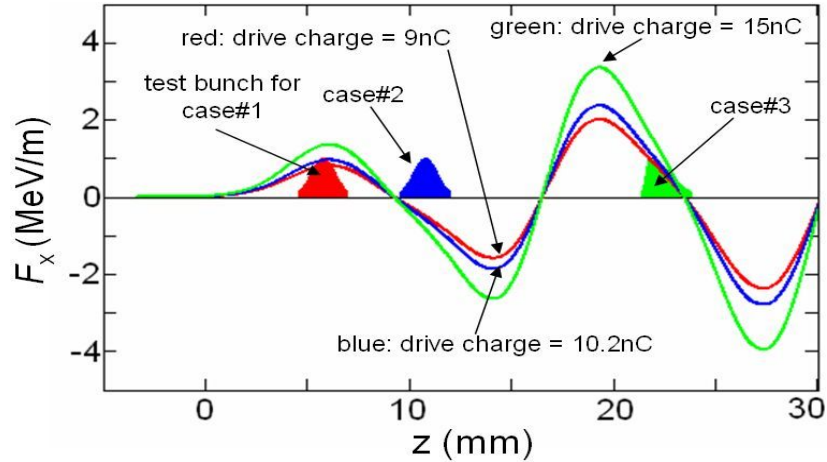


Fig. 19: $F_x(z)$ as computed by CST Studio dictates the final velocity spread and distribution; note bunches and wakefields move from right-to-left, toward lesser z -values. $F_x(z)$ –force acting on the test bunch (traveling behind the drive bunch at locations marked as case 1, or 2 or 3) is shown here computed for 9nC of the drive charge (case #1), 10.2nC of the drive charge (case #2) and 15nC (case #3). The drive bunch is off the center of its respective channel by 2mm toward the test channel. For each case the test bunch position and distribution is different, as indicated.

The angle, $\alpha_{x, \text{fin}}$, when the electron exits the apparatus is given by [again, we use the zero-order approximation in our model]:

$$\alpha_{x,fin} = \alpha_x + L \frac{F_x(z)}{E_{test}}$$

where α_x is the initial angle, $L = 100\text{mm}$ is the DWFA apparatus length, F_x (MeV/m) is computed by CST Studio and is given in Fig. 19, z is the initial position of the electron within the bunch and E_{test} is the test bunch average energy. Here we assume that the slippage between the electron and the wakefield is negligible, and energy spread is small compared to E_{test} (as it has been already confirmed by material presented before in section IV).

Thus, in this no-slippage approximation, one has $\alpha_x = \alpha_{x,fin} - L \cdot F_x(z) / E_{test}$ which allows one to trace particles to the place of their origin where the distribution is known. Hence, the final distribution becomes:

$$N_{fin}(z, \alpha_{x,fin}) = n_{of} n_{mi}(z) \exp\left(-\frac{(\alpha_{x,fin} - L F_x(z) / E_{test})^2}{2\sigma_{\alpha}^2}\right) \quad (6)$$

where all the values and parameters already have been identified on the previous pages (and n_{of} is an appropriate normalizing constant).

The final distribution in the x -velocity space is obtained by integrating the above formula over all z -values [where the beam particles can be found]; the integration is a trivial procedure when one employs MathCAD, Mathematica, or a custom C++/Fortran program. The final distribution is:

$$N_{fin}(\alpha_{x,fin}) = n_{1f} \int_z n_{mi}(z) \exp\left(-\frac{(\alpha_{x,fin} - L F_x(z) / E_{test})^2}{2\sigma_{\alpha}^2}\right) \quad (7)$$

where n_{1f} is an appropriate normalizing constant. Note that both $n_{mi}(z)$ and $F_x(z)$ depend on z , and must be integrated en-masse.

Using Eq.5 and 7 one can compare the initial and final distributions. When graphing them, it is convenient to plot

$$\begin{aligned} N_{mi}(\alpha_x) & \quad \text{vs.} \quad \alpha_x \cdot 1230\text{mm} \\ N_{fin}(\alpha_{x,fin}) & \quad \text{vs.} \quad \alpha_{x,fin} \cdot 1230\text{mm} \end{aligned}$$

because $\alpha_x \cdot 1230\text{mm}$ and $\alpha_{x,fin} \cdot 1230\text{mm}$ are the shifts (mm) one measures directly on the spectrometer screen along its X -axis [see for instance Figs 15-17, (b)]. As it has been demonstrated the theory predictions are well confirmed by the experimental observations.